# Template Synthesis of Highly Oriented Polyfluorene Nanotube Arrays†

Shane Moynihan, Daniela Iacopino, Deirdre O'Carroll, Pierre Lovera, and Gareth Redmond*

*Tyndall Institute, Lee Maltings, Prospect Row, Cork, Ireland*

*Received June 20, 2007. Revised Manuscript Received November 9, 2007*

Polyfluorene nanotubes are synthesized by solution assisted wetting of porous anodic alumina membranes. Well aligned arrays of close packed ($\sim 10^9$ tubes/cm$^{-2}$) discrete nanotubes are obtained. Individual tubes have diameters of ~260 nm and wall thicknesses of ~50 nm. X-ray diffraction measurements carried out on nanotube arrays embedded in host templates indicate a polymer chain alignment along the long axes of the template pores and, as a result, along the long axes of the nanotubes themselves. Optical spectroscopic studies of mats of nanotubes on glass substrates yield well resolved emission spectra reflecting a narrowed distribution of emitting chain segments with increased effective conjugation lengths. The data indicate intrachain reorientation of the amorphous random poly(9,9-dioctylfluorene-2,7-diyl) molecular conformation to the more planar (low energy) extended $2_1$ helical $\beta$-phase conformation within the tubes. Raman spectra acquired for template embedded tubes are also consistent with $\beta$-phase formation. Finally, polarization resolved photoluminescence data demonstrate a pronounced axial orientation of the emissive $\beta$-phase chains within the tubes.

## Introduction

The unique photophysical properties and solution processability of semiconducting polymers have made them attractive materials for fabrication of "plastic" electronic and opto-electronic devices.[1,2] At the level of individual molecules, the polymer chains exhibit intrinsically anisotropic properties, such as luminescence polarization and highly directional charge transport.[3,4] However, when conventional polymer processing methods are applied to these materials, thin films are formed in which the polymer chains are often oriented in a wide variety of conformations, creating effectively isotropic materials. One important class of semiconducting polymers is the hairy-rods. These polymers possess a rigid backbone functionalized by the attachment of flexible side chains that enhance their solubility in common organic solvents.[5] A key advantage of hairy-rods is that, on solution or melt processing, the polymers may display rich phase behavior due to the balance between unfavorable rod−coil interactions and elastic stretching of the side chains.[6] Further, when functionalized with appropriate side chains, the polymers may self-organize into nanoscale structures with regular molecular packing and alignment, thereby restoring some of the anisotropic properties of the constituent polymer molecules.[7,8]

An archetypal family of hairy-rods is that of the polyfluorene homopolymers, derivatives of poly(fluorene-2,7-diyl) bearing various substituents in the 9-position of the fluorene repeat unit.[6,9] In particular, poly(9,9-dialkylfluorene-2,7-diyl) polymers have been found to be highly efficient blue emitting materials, with high thermal and oxidative stability and with good solubility in organic solvents.[9,10] They are also liquid crystalline materials and can exist in a variety of phases by selection of appropriate material processing conditions. For example, spin casting of a poly(9,9-dioctylfluorene-2,7-diyl), PFO, thin film followed by quick solvent evaporation produces an amorphous phase of randomly oriented polymer chains.[11] On heating above ~160 °C, a nematically ordered liquid crystalline phase is formed.[12] Rapid cooling from this state yields a quenched nematic phase in which chain alignment and, as a result, anisotropic physical properties, for example, highly polarized luminescence (dichroic ratio of ~25), may be achieved.[13] Slow cooling results in a semicrystalline phase with long-range

† Part of the "Templated Materials Special Issue".

* Corresponding author. Tel: +353 4904077. Fax: +353 4270271. E-mail: gareth.redmond@tyndall.ie.

(1) Friend, R. H.; Gymer, R. W.; Holmes, A. B.; Burroughes, J. H.; Marks, R. N.; Taliani, C.; Bradley, D. D. C.; Dos Santos, D. A.; Bredas, J. L.; Salaneck, W. R. *Nature* **1999**, *397*, 121.
(2) Forrest, S. R. *Nature* **2004**, *428*, 911.
(3) Nguyen, T.-Q.; Wu, J.; Doan, V.; Schwartz, B. J.; Tolbert, S. H. *Science* **2000**, *288*, 652.
(4) Hoofman, R. J. O. M.; de Haas, M. P.; Siebbeles, L. D. A.; Warman, J. M. *Nature* **1998**, *392*, 54.
(5) Menzel, H. In *The Polymeric Materials Encyclopedia: Synthesis, Properties and Applications*; Salamone, J. C., Ed.; CRC Press: Boca Raton, FL, 1996.
(6) Knaapila, M.; Stepanyan, R.; Lyons, B. P.; Torkkeli, M.; Monkman, A. P. *Adv. Funct. Mater.* **2006**, *16*, 599.
(7) Stepanyan, R.; Subbotin, A.; Knaapila, M.; Ikkala, O.; ten Brinke, G. *Macromolecules* **2003**, *36*, 3758.
(8) Wegner, G. *Macromol. Chem. Phys.* **2003**, *204*, 347.
(9) Neher, D. *Macromol. Rapid Commun.* **2001**, *22*, 1365.
(10) Scherf, U.; List, E. J. W. *Adv. Mater.* **2002**, *14*, 477.
(11) Grell, M.; Bradley, D. D. C.; Ungar, G.; Hill, J.; Whitehead, K. S. *Macromolecules* **1999**, *32*, 5810.
(12) Grell, M.; Bradley, D. D. C.; Inbasekaran, M.; Woo, E. P. *Adv. Mater.* **1997**, *9*, 798.
(13) Misaki, M.; Ueda, Y.; Nagamatsu, S.; Yoshida, Y.; Tanigaki, N.; Yase, K. *Macromolecules* **2004**, *37*, 6926.

10.1021/cm071658f CCC: $40.75 
Published on Web 12/12/2007

order.[14] Finally, by exposing an amorphous film to, for example, toluene solvent vapor or specific thermal cycling conditions, local mechanical stresses arise within the material that cause some of the polymer chains to adopt a more planar (low energy) extended $2_1$ helical $\beta$-phase conformation.[11,15,16]

Recently, it has been shown that polyfluorene hairy-rod polymers may self-assemble into one-dimensional (1-D) fibril- and ribbon-type structures. For example, internally ordered fibril-like assemblies of poly[9,9-di-(2-ethylhexyl)-fluorenyl-2,7-diyl], PF2/6, were formed by the "photon force" of a laser beam during the drying process of a solution of the polymer in a tetrahydrofuran solution on a glass substrate.[17] Regarding the internal structure of these 1-D assemblies, observation of anisotropic luminescence from selected individual fibrils indicated that molecular orientation could be controlled by the polarization direction of the near-infrared laser beam during fibril formation. The self-assembly properties of PFO homopolymer and of a variety of block copolymers based on PFO and, for example, poly(ethylene oxide) or polystyrene, with different block ratios and molecular architectures (diblock or triblock polymers) have also been studied. Following deposition from solvents in which the compounds were dissolved, ribbon-like fibrillar objects were frequently obtained as a result of $\pi-\pi$ interactions between the conjugated segments.[18–20] Clearly, synthesis of 1-D nanostructures incorporating semiconducting hairy-rod polymers with well defined process tunable orientations will be an important step toward the realization of nanowire and nanotube based electronic and photonic devices that exhibit anisotropic electrical and optical functionalities. While the fibril formation processes highlighted above illustrate the potential for synthesis of internally oriented 1-D polyfluorene nanostructures, future applications will require the development of synthetic routes that yield large numbers of identical structures. To this end, we have recently developed methods to synthesize PFO nanowires with controlled internal morphologies. We showed that semicrystalline ($\alpha$-phase) PFO nanowires with regular end facets may be formed by melt-assisted template wetting and that this approach allows nanowire active waveguiding, Fabry-Pérot microcavity behavior, and optically pumped lasing to be achieved.[21–23]

In this paper, we report on the first synthesis of polyfluorene nanotubes by the method of wetting of porous anodic alumina membrane templates. This method has previously been shown to be capable of efficiently forming nanotubes for a range of organic materials, for example, small molecules, oligomers, polymers, blends, and multicomponent solutions, with good control over the nanotube diameter, length, wall thickness, and areal density.[24–28] Filling of the alumina template pores by polymer solution is thought to occur by a wetting process whereby an extremely thin precursor film, emanating from a macroscopic polymer solution droplet, rapidly covers the template surface.[24] Wetting is driven by short- and long-range van der Waals interactions between the low surface energy wetting liquid and the high surface energy pore walls. After the wetting layer has formed, these strong adhesive forces are neutralized. Evaporation of the carrier solvent at this point then results in trapping of the polymer material as nanotubes within the template pores. Using this approach, we synthesized aligned arrays of close packed PFO nanotubes. Individual PFO tubes were found to have diameters of ~260 nm and wall thicknesses of ~50 nm. X-ray diffraction (XRD) measurements carried out on nanotube arrays embedded in oxide templates indicated polymer chain alignment along the long axes of the template pores and, as a consequence, along the long axes of the nanotubes themselves. Optical spectroscopic studies of nanotube mats deposited onto glass substrates from aqueous suspensions yielded well resolved photoluminescence (PL) spectra that reflected a narrowed distribution of emitting chain segments with increased effective conjugation lengths. The data was indicative of intrachain reorientation of the amorphous random PFO molecular conformation to the more planar (low energy) extended $2_1$ helical $\beta$-phase conformation within the nanotubes. Raman spectra acquired for template embedded nanotubes were consistent with the formation of the planarized, extended $\beta$-phase conformation. Finally, polarization resolved PL data demonstrated a pronounced axial alignment of the emissive $\beta$-phase chains within the tubes.

## Experimental Section

**Materials.** PFO with a polydispersity index of 2.9 and a mean molecular weight, MW, of 64 000 g/mol was purchased from American Dye Source, Inc., and stored under nitrogen before use. Porous anodized alumina membranes (Anodisc 25, 200 nm nominal pore diameter) were purchased from Whatman Ltd. Decane was purchased from Fluka, while all other reagents and solvents were purchased from Aldrich and were used without further purification. Deionized water (Millipore Q, >18 MΩ cm) was used for all aqueous solutions.

**Nanotube Synthesis.** Nanotubes were fabricated under ambient conditions using the technique of solution assisted template wetting: 80 $\mu$L of a PFO solution in tetrahydrofuran (THF, 40 mg/mL) was drop deposited onto a glass microscope slide. An alumina membrane

(14) Chen, S. H.; Su, A. C.; Su, C. H.; Chen, S. A. *Macromolecules* **2005**, *38*, 379.
(15) Ariu, M.; Lidzey, D. G.; Sims, M.; Cadby, A. J.; Lane, P. A.; Bradley, D. D. C. *J. Phys.: Condens. Matter* **2002**, *14*, 9975.
(16) Ariu, M.; Lidzey, D. G.; Bradley, D. D. C. *Synth. Met.* **2000**, *111*, 607.
(17) Masuo, S.; Yoshikawa, H.; Nothofer, H.-G.; Grimsdale, A. C.; Scherf, U.; Müllen, K.; Masuhara, H. *J. Phys. Chem. B* **2005**, *109*, 6917.
(18) Leclère, P.; Hennebicq, E.; Calderone, A.; Brocorens, P.; Grimsdale, A. C.; Müllen, K.; Brédas, J. L.; Lazzaroni, R. *Prog. Polym. Sci.* **2003**, *28*, 55.
(19) Surin, M.; Hennebicq, E.; Ego, C.; Marsitzky, D.; Grinsdale, A. C.; Müllen, K.; Brédas, J. L.; Lazzaroni, R.; Leclère, P. *Chem. Mater.* **2004**, *16*, 994.
(20) Surin, M.; Marsitzky, D.; Grinsdale, A. C.; Müllen, K.; Lazzaroni, R.; Leclère, P. *Adv. Funct. Mater.* **2004**, *14*, 708.
(21) O'Carroll, D.; Redmond, G. *Small* **2007**, *3*, 1178.
(22) O'Carroll, D.; Redmond, G. *Physica E*, in press.
(23) O'Carroll, D.; Lieberwirth, I.; Redmond, G. *Nat. Nanotechnol.* **2007**, *2*, 180.
(24) Steinhart, M.; Wehrspohn, R. B.; Gösele, U.; Wendorff, J. H. *Angew. Chem., Int. Ed.* **2004**, *43*, 1334.
(25) Hulteen, J. C.; Martin, C. R. *J. Mater. Chem.* **1997**, *7*, 1075.
(26) Barrett, C.; Iacopino, D.; O'Carroll, D.; De Marzi, G.; Tanner, D. A.; Quinn, A. J.; Redmond, G. *Chem. Mater.* **2007**, *19*, 338.
(27) Moynihan, S.; Iacopino, D.; O'Carroll, D.; Doyle, H.; Tanner, D. A.; Redmond, G. *Adv. Mater.* **2007**, *19*, 2474.
(28) Steinhart, M.; Senz, S.; Wehrspohn, R. B.; Gösele, U.; Wendorff, J. H. *Macromolecules* **2003**, *36*, 3646.

was placed on top of the drop, which was then covered by another glass microscope slide. Pressure of approximately 50 kPa was applied over a period of 15 h. After drying, excess polymer was removed from both sides of the membrane using a scalpel, followed by polishing with 1200 grid sand paper. Nanotubes were freed by soaking the membrane in 3 M aqueous NaOH for 5 h. The tube material was extracted from the resulting mixture by three cycles of centrifugation (8000 rpm, 30 s), supernatant removal, and redispersion in 3 M aqueous NaOH (manual agitation), followed by two more cycles in water. Tubes were then dispersed in decane or water by sonication.

**Nanotube Imaging.** Scanning electron microscopy (SEM) images of PFO nanotubes embedded in alumina templates and of freestanding tube arrays were acquired using a field emission instrument (JSM-6700F, JEOL U.K. Ltd.) operating at beam voltages of 3–5 kV. To confirm tube formation, nanotube arrays in polished alumina templates were embedded in paraffin wax ($T_m \sim$ 56 °C, Raymond A. Lamb Inc.) and sectioned by microtomy (1512 rotary microtome, Leitz Wetzlar GmbH). Sections were collected, dis-embedded by using a scalpel to remove excess wax and dissolving the remaining wax in *o*-xylene, washed with $H_2O$, and dried. Prior to imaging, membrane samples were cleaned and mounted onto SEM stubs using adhesive carbon pads. To image freestanding nanotube arrays, a filled membrane, mounted as indicated above, was dipped into 3 M aqueous NaOH for 2 h to dissolve the alumina host and leave freestanding "forests" of PFO tubes. Samples were coated with gold to facilitate SEM imaging (Scancoat Six sputter coater, 30 mA, 0.2 torr, 60 s). Individual nanotubes, drop deposited onto gold-coated silicon wafer substrates from aqueous suspension, were also imaged (10 kV beam voltage). The topography of the isolated nanotubes drop deposited onto acid cleaned glass substrates (30 min MeOH/HCl 1:1 v/v, 30 min $H_2SO_4$, $H_2O$ rinse) was also characterized using a calibrated atomic force microscope (AFM; Topometrix Explorer, Veeco Instruments Ltd.) using noncontact mode silicon tips (1650-00, Veeco Instruments Ltd., tip radius $<$ 10 nm).

**Nanotube Structural Characterization.** XRD measurements were performed using an X'Pert PRO diffractometer (PANalytical Ltd., U.K.) in symmetric reflection coupled $\theta/2\theta$ mode with Cu K$\alpha$ radiation ($\lambda_{K\alpha} = 1.549$ Å), a step size of 0.02°, and a scan integration time of 50 s/step. Each sample was placed into the diffractometer so that its top surface was perpendicular to the plane defined by the incident and scattered X-ray beams. $\psi$-scans were acquired for fixed values of $\theta/2\theta$ with a step size of 0.5° and an integration time of 50 s/step.

**Nanotube Spectroscopy.** Raman spectra of PFO thin films and nanotube arrays embedded in polished alumina templates were recorded using a Raman imaging microscope (Renishaw Plc.). Pristine thin films (50 nm thickness) were prepared by spin-casting a 7 mg/mL PFO solution in THF onto thermally oxidized silicon wafer substrates (6000 rpm, 60 s). Samples were excited by the 514 nm line of an argon-ion laser. As this wavelength was close to the PFO absorption onset, some background PFO luminescence was found to be present in the measured spectra. All spectra were therefore normalized by baseline fitting and subtraction. Spectra were also referenced to the Si 518 nm peak.

PL spectra of PFO solutions, thin films, and nanotubes were acquired using a home-built system. Samples were optically pumped at 350 nm by an argon ion laser (Innova Enterprise II, Coherent Inc.) using reflective neutral density filters (Newport Corp.) to attenuate the excitation intensity. Emission spectra of the solutions were acquired by focusing the pump light into a quartz cuvette and collecting the emission at 90°. Spectra of the thin films and nanotube mats were acquired by focusing the pump light onto the samples at an angle of 27° to the plane of the sample with a spot size of $\sim 2 \times 8$ mm and collecting the resultant emission at an angle of 63°. In all cases, suitable long pass filters were used for emission collection (Glen Spectra Ltd.). Emitted light was directed to a Triax 190 0.19 m monochromator (1200 lines/mm, 500 nm blaze, Horiba Jobin Yvon Ltd.) via an optical fiber bundle. Spectra were recorded at an integration time of 0.1 s using a Hamamatsu R928 photomultiplier (Hamamatsu Photonics U.K. Ltd.). Polarization dependent spectra of nanotube arrays in alumina templates were also acquired by focusing the pump light onto the samples at an input angle of 15° to the plane of the template surface while emission was detected at an angle of 10°. Excitation polarization was set using a half-wave plate, and collection polarization was selected using a Glan-Thompson polarizer (Thorlabs Inc.). Emission collection via the fiber bundle ensured that the light was depolarized prior to entering the monochromator thereby avoiding possible transmission bias associated with the vertically ruled grating.

## Results and Discussion

The objective of this paper was to demonstrate synthesis of polyfluorene nanotubes using the method of solution assisted template wetting and to explore the resulting structural and optical properties of these novel nanostructures. In this regard, PFO, a highly efficient blue emitting polymer with high thermal and oxidative stability and with good solubility in organic solvents, was selected.[9] PFO was considered as a particularly interesting candidate for nanotube formation because it is a polymorphic liquid crystalline material which can exist in a variety of phases depending on the processing history.[11] PFO nanotubes were fabricated using a template molding technique. Briefly, a droplet of PFO solution in THF was dispensed onto a clean glass slide, and a porous anodized alumina membrane was then placed on top of this droplet. The membrane was then sandwiched by another glass microscope slide, and pressure was applied. After solvent evaporation, excess polymer was removed from the external surfaces of the alumina membrane by polishing yielding arrays of PFO nanotubes embedded within the template.

Pristine (unfilled) alumina templates were imaged using SEM; see Figure 1a. The nanoporous structure of the membranes was apparent, with straight parallel pores penetrating through the alumina material. Statistical analysis indicated that the long axes of these pores were arranged in a Gaussian distribution of orientations about the axis normal to the membrane template surface with a standard deviation of $\sim$2°; that is, the pores were very well aligned almost normal to the template surface and parallel to one another. Membrane thickness was also measured as $\sim$56 $\mu$m, in good accordance with the stated nominal value of 60 $\mu$m. Figure 1b shows an SEM image of a typical piece of alumina membrane that had been sectioned by microtomy following nanotube synthesis. The image clearly shows the presence of the polymer nanotubes embedded within the membrane template.

Following synthesis, the membrane template material could be selectively removed by soaking in aqueous NaOH. Figure 1c shows an SEM image of a freestanding array of PFO nanotubes following dissolution of a filled template, confirming that well aligned forests of close-packed high

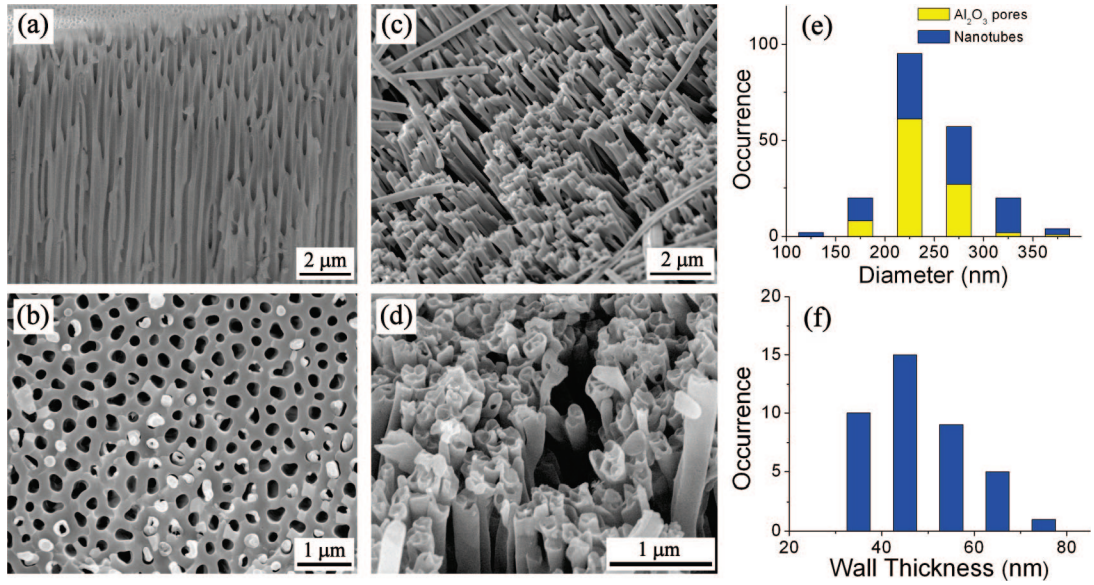


**Figure 1.** SEM images of (a) a pristine alumina template, (b) a section through a template showing embedded PFO nanotubes, (c) a PFO nanotube array following template removal, and (d) a PFO nanotube array at high magnification. Histograms of (e) pore mouth diameters of alumina membranes (yellow) and external diameters of PFO nanotubes (blue) and (f) nanotube wall thicknesses.

aspect ratio 1-D nanostructures could be obtained at high yields ($\sim 10^9$ tubes per membrane). High magnification SEM imaging of the nanostructures indicated that they had tubular morphology with smooth side walls; see Figure 1d. The relationship between the template pore dimensions and the corresponding dimensions of the nanotubes synthesized within the pores was investigated. For pristine membranes, the frequency distribution of pore mouth diameters (total pore count = 100) was estimated by statistical analysis of the SEM images; see Figure 1e, yellow bars. The data suggested that the template pores had diameters of 244 ± 48 nm, that is, slightly larger than the manufacturer's stated nominal value of 200 nm. The external diameters of PFO nanotubes were likewise analyzed and plotted as a frequency distribution (total count = 100); see Figure 1e, blue bars. The data indicated that the nanotubes had diameters of 257 ± 83 nm with a frequency distribution similar to that of the template pore diameters, indicating a correlation between the template and the nanotube critical dimensions. In addition, Figure 1f shows a frequency distribution of PFO nanotube wall thicknesses estimated by statistical analysis of the SEM image data for freestanding arrays. A wall thickness of 50 ± 18 nm was obtained.

To further purify the nanotubes, multiple cycles of centrifugation, supernatant removal, and redispersion by agitation were employed to separate discrete tubes from dissolved or particulate template material. Extracted nanotubes were finally dispersed in decane or water by sonication. Figure 2a shows an SEM image of a typical isolated nanotube deposited onto a gold coated silicon wafer from a decane dispersion. The data indicated that the nanotubes had a smooth tubular morphology, with this particular tube having a diameter of ~260 nm and a wall thickness of ~40 nm. Figure 2b shows a noncontact mode AFM image of two nanotubes deposited onto an acid cleaned glass slide from an aqueous dispersion. In this case, the tube ends had split and unfurled, likely as a result of the effects of sonication

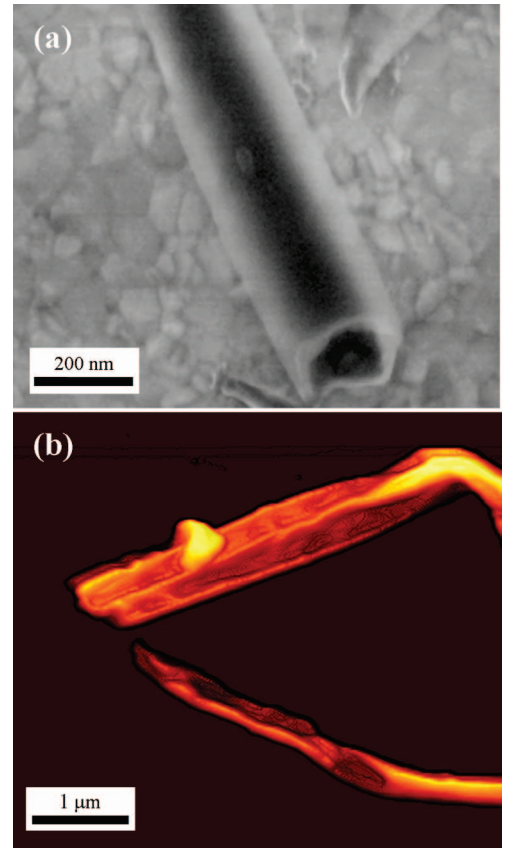


**Figure 2.** (a) High magnification SEM image of an isolated PFO nanotube on a gold coated silicon substrate. (b) Noncontact mode AFM image of the split ends of two PFO nanotubes on a glass substrate.

during dispersion. Topographic line profiles of this sample indicated wall thicknesses of 50–70 nm, in good agreement with values estimated by analysis of the SEM image data.

To obtain information regarding the nature and extent of molecular organization within the nanotube arrays, XRD data were acquired for pristine alumina membrane templates and for PFO nanotube arrays embedded in polished alumina

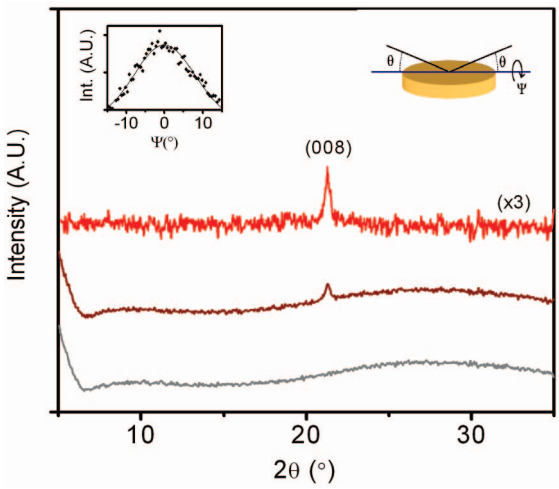


**Figure 3.** X-ray diffractograms acquired for an empty alumina template background (gray line) and a PFO nanotube array embedded in a polished alumina template (brown line). Background subtracted data for an array is also shown (red line). Right inset: schematic representation of the measurement configuration. Left inset: plot of (008) peak intensity as a function of template tilt angle, $\psi$, (solid diamonds) with a single Gaussian fit to the data (solid line).

templates. Each membrane was fixed into the diffractometer such that the template surface was oriented normal to the plane defined by the incident and scattered X-ray beams; see Figure 3, right inset. Diffractograms acquired for pristine alumina templates did not exhibit any reflections in the scan range employed; see, for example, Figure 3, gray line. However, diffractograms acquired for nanotube arrays were characterized by a single sharp peak at 21.27° 2$\theta$, corresponding to the (008) reflection of PFO; see, for example, Figure 3, brown line. Background subtraction from the nanotube data indicated that the (008) reflection was typically superimposed on a broad halo centered at ~20° 2$\theta$; see Figure 3, red line. The (008) reflection indicated a $d$ spacing of 4.2 Å and corresponded to the phenyl-ring repeat distance on the polymer backbone (i.e., half of the fluorene monomer periodic distance).[29] The intensity and sharpness of this peak suggested that some of the PFO chains within the nanotubes were aligned normal to the template surface. The absence of any other peaks indicated a lack of interchain registry between the PFO chains.[30] The broad halo was attributed to short-range intra and interchain order, suggesting that the aligned polymer chains were embedded within an amorphous polymer matrix.[31]

Rocking angle $\psi$ scans were then performed to quantify the extent of the polymer chain alignment within the nanotube arrays. The incident beam and detector angles were fixed at values corresponding to the maximum intensity of the (008) peak, that is, 21.3° 2$\theta$. Each nanotube filled membrane was then tilted by $\psi$, the angle between the template surface normal and the plane defined by the incident and scattered X-ray beams; see Figure 3, right inset. The variation of intensity with $\psi$ was measured for each sample. Intensity profiles were typically characterized by a maximum at $\psi = 0°$ and a full width at half-maximum of 19°; see, for example, Figure 3, left inset. Single Gaussian fits to such data indicated that the polymer chains were arranged in a distribution of orientations about the template surface normal with a standard deviation, $\sigma$, of 8°. Hence, the measured data confirmed that a significant fraction of the PFO polymer molecules within the nanotubes were very well aligned, being axially oriented along the template pores and, by extension, along the nanotubes themselves.

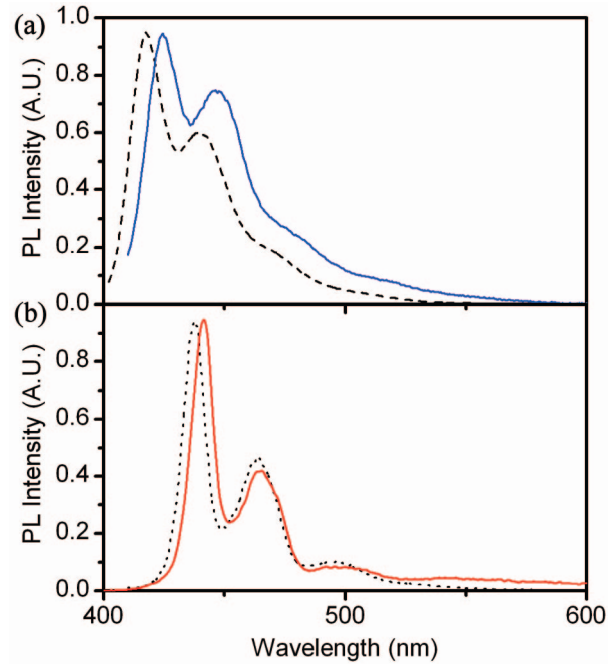


**Figure 4.** (a) PL spectra acquired for an 8 $\mu$g/mL PFO solution in THF (dashed black line) and for an amorphous PFO thin film spin cast onto a glass substrate from a chloroform solution (solid blue line). (b) PL spectra acquired for the same film following toluene vapor exposure (dotted black line) and for a mat of PFO nanotubes drop deposited onto a glass substrate from an aqueous suspension (solid red line).

To explore whether any changes in PFO internal morphology occurred during nanotube synthesis, PL spectra were measured for various PFO samples. A typical emission spectrum acquired for an 8 $\mu$g/mL solution of PFO in THF is shown in Figure 4a, black dashed line. This spectrum exhibited a characteristic vibronic progression with peaks located at 417, 440, 470, and ~510 nm arising from the $S_1 \rightarrow S_0$ 0-0 singlet exciton transition of PFO with 0-1, 0-2, and 0-3 vibronic replicas, respectively. By comparison, the emission spectrum of a PFO thin film prepared by spin casting onto a glass substrate from a chloroform solution (20 mg/mL, 3500 rpm, 60 s) exhibited peaks at 432, 452, 478, and ~520 nm characteristic of amorphous phase PFO; see Figure 4a, blue line. This spectrum was red-shifted with respect to the solution spectrum by ~15 nm, likely because of an increase in the dielectric constant of the environment around each chromophore as well as increased Förster energy transfer between nearby chromophores in the solid film. The

(29) Kawana, S.; Durrell, M.; Lu, J.; McDonald, J. E.; Grell, M.; Bradley, D. D. C.; Jukes, P. C.; Jones, R. A. L.; Bennett, S. L. *Polymer* **2002**, *43*, 1907.
(30) Wang, X.-J.; Zhou, Q.-F. *Liquid Crystalline Polymer*; World Scientific Publishing Co. Pte. Ltd.: Singapore, 2004.
(31) Knaapila, M.; Ikkala, O.; Torkkeli, M.; Jokela, K.; Serimaa, R.; Dolbnya, I. P.; Bras, W.; ten Brinke, G.; Horsburgh, L. E.; Pålsson, L.-O.; Monkman, A. P. *Appl. Phys. Lett.* **2002**, *81*, 1489.

latter effect would favor transfer of energy to, and luminescence from, longer lower energy polymer segments.[32]

When this film was exposed to toluene vapor (10 min), the resulting measured emission spectrum exhibited further red-shifted and significantly narrower emission peaks (at 438, 464, 498, and ~535 nm); see Figure 4b, black dotted line. The spectrum indicated a narrowed distribution of emitting chain segments with increased effective conjugation lengths and was attributed to intrachain reorientation of the amorphous random PFO molecular conformation to the more planar (low energy) extended $2_1$ helical $\beta$-phase conformation.[15] Upon photoexcitation, efficient Förster energy transfer from the amorphous host matrix to the lower energy $\beta$-phase (Förster radius ~ 8.2 nm) is known to occur, aided by good intermixing between the two phases and significant overlap between amorphous phase emission and $\beta$-phase absorption spectra.[32] Consequently, the emission spectra of such samples are dominated by the $\beta$-phase. An emission spectrum acquired for a mat of PFO nanotubes deposited onto a glass substrate from an $H_2O$ suspension is shown in Figure 4b, red line. Interestingly, this spectrum also exhibited a vibronic progression with peaks at 441, 465, 499, and ~539 nm characteristic of the planarized elongated $\beta$-phase. The spectrum was red-shifted with respect to that of the solvent treated film possibly as a result of a further increase in effective conjugation lengths due to greater polymer chain extension within the nanotubes.[32] $\beta$-phase formation in the PFO nanotubes was attributed to the action of mechanical stresses that arose within the polymer during solution assisted filling of the template pores and, afterward, during the evaporation of the solvent from the pores.

Raman scattering studies of conjugated polymers yield information on local backbone and side-chain conformations of polymer molecules. To gain further insight into the composition and internal structure of the PFO nanotubes, Raman spectra were acquired for PFO thin films and compared with spectra acquired for nanotube arrays. Amorphous PFO films were first prepared by spin casting onto silicon wafer substrates from a THF solution (7 mg/mL, 6000 rpm, 60 s).[11] Raman spectra were characterized by a single intense high frequency peak, at 1605 $cm^{-1}$, and multiple less intense lower frequency peaks in the 1500 to 1100 $cm^{-1}$ range; see Figure 5, blue lines. The prominent high frequency peak is typically observed for conjugated polymers that incorporate phenyl rings in their backbone and, in PFO in particular, it has been attributed to a symmetric intraphenyl ring C−C stretching mode.[32,16] The lower frequency peaks between 1350 and 1250 $cm^{-1}$ are known to be associated with interphenyl ring backbone C−C stretching modes. In PFO, modes associated with C−C stretching in the same monomeric unit occur at higher energies than those associated with C−C stretching between adjacent monomer units. The peaks between 1250 and 1170 $cm^{-1}$ and between 1170 and 1110 $cm^{-1}$ have been attributed to C−H bending modes of the backbone and side chains, respectively.[33,16]

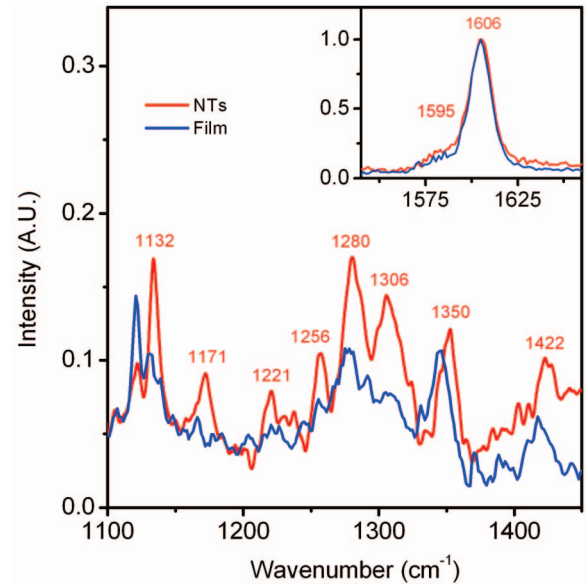


**Figure 5.** Raman spectra of a PFO thin film spin cast onto a silicon substrate (blue line) and of a PFO nanotube array embedded in a polished alumina membrane template (red line).

Raman spectra of PFO nanotube arrays embedded within polished alumina membrane templates were then acquired; see Figure 5, red lines. These spectra also typically exhibited a single intense high frequency peak and a number of lower frequency peaks in the 1500 to 1100 $cm^{-1}$ range. Concerning the position of the high frequency peak, a slight energy shift of this symmetric ring stretching mode to 1606 $cm^{-1}$, that is, hardening, with respect to that of the spin cast film occurred. This shift was similar to behavior predicted following synthetic incorporation of interphenyl bridges into helical poly(p-phenylene) (PPP) to convert it to its more planar "ladder type" (LPPP) form.[34] Such a change suggested a slight stretching of PFO molecular backbones within the nanotubes, possibly because of polymer chain planarization. Concerning spectral features in the 1500 to 1100 $cm^{-1}$ range, peaks associated with interphenyl ring backbone stretching and C−H bending modes exhibited slight hardening, some sharpening, and pronounced intensity enhancement (relative to the main 1606 $cm^{-1}$ mode). For polyfluorenes, peak hardening and intensity enhancement are usually associated with planarization of the polymer molecules.[33] Very similar changes have been reported for Raman spectra of amorphous PFO thin films following solvent vapor treatment to generate $\beta$-phase fractions.[16] Hence, the Raman spectral changes observed for the PFO nanotubes were attributed to the formation of the planarized extended $\beta$-phase conformation within the nanotubes.

To explore whether the $\beta$-phase emitters adopted any specific orientation or alignment within the PFO nanotubes, polarization resolved PL spectroscopy measurements of nanotube arrays embedded in polished alumina templates were undertaken. To acquire polarization dependent spectra, each membrane was fixed into the spectrometer such that the template surface normal was oriented horizontally with

(32) Ariu, M.; Sims, M.; Rahn, M. D.; Hill, J.; Fox, A. M.; Lidzey, D. G.; Oda, M.; Cabanillas-Gonzalez, J.; Bradley, D. D. C. *Phys. Rev. B* **2003**, *67*, 195333.
(33) Tanto, B.; Guha, S.; Martin, C. M.; Scherf, U.; Winokur, M. J. *Macromolecules* **2004**, *37*, 9438.
(34) Cuff, L.; Kertesz, M. *J. Phys. Chem.* **1994**, *98*, 12223.
(35) Chen, S. H.; Su, A. C.; Chen, S. A. *J. Phys. Chem. B* **2005**, *109*, 10067.

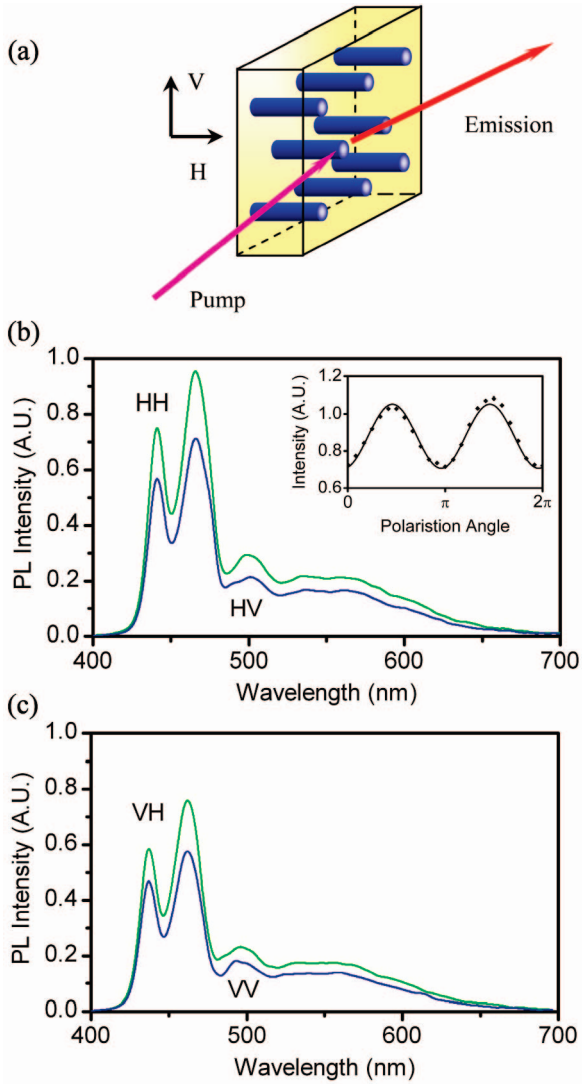


**Figure 6.** (a) Schematic representation of the setup used for polarization resolved PL measurements on PFO nanotube arrays embedded in polished alumina templates. (b) PL spectra of a nanotube array acquired under horizontal excitation polarization with horizontal (HH, green line) and vertical (HV, navy line) detection polarizations, respectively. Inset: plot of emission intensity vs detection angle ($\theta$) with least-squares $\sin^2\theta$ fit. (c) PL spectra of the array acquired under vertical excitation polarization with horizontal (VH, green line) and vertical (VV, navy line) detection polarizations, respectively.

respect to the laboratory reference frame. Excitation light was focused onto the sample at an angle of 15° to the plane of the template surface while emission was collected at an angle of 10° to the plane; see Figure 6a. A half-wave plate and a Glan-Thomson polarizer were employed to control the polarizations of the excitation light and the detected light, respectively. Horizontally polarized light had a polarity normal to the template surface, while vertically polarized light had a polarity parallel to the template surface. Typical polarization resolved PL spectra are shown in Figure 6b,c. These spectra exhibited characteristically red-shifted and narrowed emission peaks at 441, 466, 503, and ~540 nm that were assigned to the 0-0, 0-1, 0-2, and 0-3 singlet exciton transitions of $\beta$-phase PFO. The nanotube array spectra exhibited greater relative attenuation of the 0-0 peak compared with the nanotube mat spectra of Figure 4b, consistent with the increased self-absorption occurring at these wavelengths within the ~56 $\mu$m thick nanotube filled membrane.[35]

Concerning the polarization dependence of the PL data, the spectra of Figure 6b were acquired under conditions of horizontally polarized excitation with horizontally (HH) or vertically (HV) polarized detection, respectively. This data indicated that the measured PL intensity was maximal under conditions of horizontally polarized detection. The data shown in the inset to Figure 6b also reflects this trend. This plot of 0-1 emission peak intensity versus detection polarization, acquired under horizontally polarized excitation conditions, followed a $\sin^2\theta$ relationship, indicating reproducible polarization dependent behavior, with emission intensity maxima occurring when the detection polarization was normal to the template surface. The spectra of Figure 6c were acquired under conditions of vertically polarized excitation with horizontally (VH) or vertically (VV) polarized detection, respectively. Once again, this data indicated that the measured PL intensity was maximal under conditions of horizontally polarized detection; that is, despite the fact that the sample was excited with vertically polarized light, emission had a preferred horizontal polarization. Therefore, regardless of excitation polarization, emission from the PFO nanotube array was preferentially horizontally polarized. This indicated that some of the $\beta$-phase emitters were well aligned along the long axes of the template pores and, consequently, along the long axes of the nanotubes themselves.

However, despite the distinct PL anisotropy of the nanotube arrays, considerable vertically polarized emission was detected throughout the measurements. The presence of detected light with this polarization may be attributed to one or more of the following factors. (i) In PFO, the emission transition dipole is oriented at ~26.5° off the physical axis of the polymer molecular backbone.[36] This off-axis angle will tend to reduce any measured PL anisotropy. (ii) In the solid state, excitations may migrate between PFO chain segments with varying orientations.[37] Such energy transfer processes would provide another source of polarization loss. (iii) Strong light scattering by the templates could reduce polarization anisotropy. (iv) Randomly organized residual polymer material on the template surfaces could contain a broad distribution of emitter orientations. Because care was taken to ensure that templates were as clean as possible, this factor was not considered to be of major importance. Taken together, the polarization resolved PL data indicated that nanotube array emission originated from planarized, elongated $2_1$ helical $\beta$-phase emitters and that a significant fraction of these chains was axially aligned within the tubes.

## Conclusions

In summary, polyfluorene nanotubes have been synthesized by solution assisted wetting of porous anodic alumina membranes. Well aligned arrays of close packed (~$10^9$ tubes/$cm^{-2}$) discrete nanotubes were obtained. Individual tubes

(36) Liem, H.-M.; Etchegoin, P.; Whitehead, K. S.; Bradley, D. D. C. *Adv. Funct. Mater.* **2003**, *13*, 66.
(37) Schartel, B.; Wachtendorf, V.; Grell, M.; Bradley, D. D. C.; Hennecke, M. *Phys. Rev. B* **1999**, *60*, 277.

were found to have diameters of ~260 nm and wall thicknesses of ~50 nm. XRD measurements carried out on nanotube arrays embedded in oxide templates indicated polymer chain alignment along the long axes of the template pores and, as a consequence, along the long axes of the nanotubes themselves. Optical spectroscopic studies of nanotube mats deposited onto glass substrates from aqueous suspensions yielded well resolved PL spectra that reflected a narrowed distribution of emitting chain segments with increased effective conjugation lengths. The data was indicative of intrachain reorientation of the amorphous random PFO molecular conformation to a more planar (low energy) extended $2_1$ helical $\beta$-phase conformation within the nanotubes. Raman spectra acquired for template embedded nanotubes were consistent with the formation of the planarized extended $\beta$-phase conformation. Finally, polarization resolved PL data demonstrated a pronounced axial alignment of the emissive $\beta$-phase chains within the tubes. The ability to synthesize 1-D nanostructures with well defined structural and optical properties based on semiconducting hairy-rod polymers such as polyfluorene in this manner should be a useful step toward the realization of future polymer based nanowire and nanotube opto-electronic devices with tailored functionalities.

**Acknowledgment.** The authors thank Dr. Selena O'Keeffe for help with sample microtomy. The support of the Irish Government HEA PRTLI Nanoscience Initiative and of the European Union "Nano3D" project is also gratefully acknowledged.

CM071658F